AGU PUBLICATIONS

JGR

Journal of Geophysical Research: Atmospheres

RESEARCH ARTICLE

10.1002/2017JD027691

Simulated Historical (1901–2010) Changes in the Permafrost Extent and Active Layer Thickness in the Northern Hemisphere

Donglin Guo[1,2,3] **and Huijun Wang**[2]

[1]Nansen-Zhu International Research Centre, Institute of Atmospheric Physics, Chinese Academy of Sciences, Beijing, China, [2]Key Laboratory of Meteorological Disaster, Ministry of Education/Collaborative Innovation Center on Forecast and Evaluation of Meteorological Disasters, Nanjing University of Information Science and Technology, Nanjing, China, [3]Joint Laboratory for Climate and Environmental Change, Chengdu University of Information Technology, Chengdu, China

Key Points:
- Long-term observations of changes in soil temperature and active layer thickness confirm that simulations using the CLM4.5 driven by the CRUNCEP data set give reasonable results
- Permafrost is sensitive to the short-term warming seen in the 1930s and the 1940s
- Regional differences in the rate of historical thawing of permafrost are mostly linked to the sensitivity of permafrost in the regions to increases in air temperature rather than the amplitude of the temperature increases

Correspondence to:
D. Guo,
guodl@mail.iap.ac.cn

Citation:
Guo, D., & Wang, H. (2017). Simulated historical (1901–2010) changes in the permafrost extent and active layer thickness in the Northern Hemisphere. *Journal of Geophysical Research: Atmospheres*, *122*, 12,285–12,295. https://doi.org/10.1002/2017JD027691

Received 1 SEP 2017
Accepted 4 NOV 2017
Accepted article online 8 NOV 2017
Published online 24 NOV 2017

Abstract A growing body of simulation research has considered the dynamics of permafrost, which has an important role in the climate system of a warming world. Previous studies have concentrated on the future degradation of permafrost based on global climate models (GCMs) or data from GCMs. An accurate estimation of historical changes in permafrost is required to understand the relations between changes in permafrost and the Earth's climate and to validate the results from GCMs. Using the Community Land Model 4.5 driven by the Climate Research Unit -National Centers for Environmental Prediction (CRUNCEP) atmospheric data set and observations of changes in soil temperature and active layer thickness and present-day areal extent of permafrost, this study investigated the changes in permafrost in the Northern Hemisphere from 1901 to 2010. The results showed that the model can reproduce the interannual variations in the observed soil temperature and active layer thickness. The simulated area of present-day permafrost fits well with observations, with a bias of 2.02×10^6 km^2. The area of permafrost decreased by 0.06 (0.62) $\times 10^6$ km^2 decade^{-1} from 1901 to 2009 (1979 to 2009). A clear decrease in the area of permafrost was found in response to increases in air temperatures during the period from about the 1930s to the 1940s, indicating that permafrost is sensitive to even a temporary increase in temperature. From a regional perspective, high-elevation permafrost decreases at a faster rate than high-latitude permafrost; permafrost in China shows the fastest rate of decrease, followed by Alaska, Russia, and Canada. Discrepancies in the rate of decrease in the extent of permafrost among different regions were mostly linked to the sensitivity of permafrost in the regions to increases in air temperatures rather than to the amplitude of the increase in air temperatures. An increase in the active layer thickness of 0.009 (0.071) m decade^{-1} was shown during the period of 1901–2009 (1979–2009). These results are useful in understanding the response of permafrost to a historical warming climate and for validating the results from GCMs.

1. Introduction

Permafrost occupies approximately 25% of the land area of the Northern Hemisphere. It is estimated that approximately 1,830 Pg of soil organic carbon is stored in permafrost soils, equivalent to approximately 2.2 times more carbon than is present in the Earth's current atmosphere (Ciais et al., 2013; Mu et al., 2015). Zhang et al. (1999) estimated that approximately 11.4–36.6 $\times 10^3$ km^3 of ground ice is stored in permafrost in the Northern Hemisphere. In addition, large populations and engineering facilities have expanded into permafrost regions in recent decades as a result of their abundant natural resources in these regions (Nelson, Anisimov, & Shiklomanov, 2002). Seasonally freezing and thawing processes in the active layer of permafrost are closely related to the surface ecology, hydrology, and energy budget of these regions (Cuo et al., 2015; Guo, Yang, & Wang, 2011a, 2011b; Yi et al., 2014). Permafrost has a large sensitivity to climate change and is distributed in regions with the greatest recorded warming, which makes it likely that permafrost will begin to thaw in response to global climate change (Collins et al., 2013; Guo et al., 2017; Guo & Wang, 2012; Tian & Jiang, 2015; Zhou et al., 2016). The thawing of permafrost can result in the release of soil organic carbon, the melting of ground ice, and changes in the seasonal soil freezing and thawing processes. These changes will, in turn, affect the climate (Li & Chen, 2013; Schuur et al., 2015), the hydrology and availability of water resources (Guo, Wang, & Li, 2012; Liljedahl et al., 2016), the stabilization of engineering facilities underlain by permafrost (Guo & Sun, 2015; Guo & Wang, 2016b; Nelson et al., 2002), and the terrestrial ecosystem (Qin, Zhou, & Xiao, 2014; Yang et al., 2010). Therefore permafrost has an important role in the climate system of a warming world.

A growing body of research has simulated the potential thawing of permafrost (Anisimov & Nelson, 1996; Guo & Wang, 2013; Guo & Wang, 2016a; Koven, Riley, & Stern, 2013; Lawrence et al., 2011, 2008; Liu & Jiang, 2016; Slater & Lawrence, 2013; Stendel & Christensen, 2002; Zhang, Chen, & Riseborough, 2008). An early simulation using a diagnostic model in conjunction with data from three global climate models (GCMs) suggested a reduction of 25–44% in the area of permafrost in response to a 2°C increase in global temperatures (Anisimov & Nelson, 1996). Reductions in permafrost area of 33% (Representative Concentration Pathway (RCP) 2.6), 49% (RCP4.5), 62% (RCP6.0), and 72% (RCP8.5) were also projected using the fully coupled Community Climate System Model, version 4.0 (Lawrence et al., 2012). More recently, multiple GCMs or data from multiple GCMs have been used to estimate future permafrost variation and the results have suggested that the area of permafrost will decrease by 37 ± 11% (RCP2.6), 51 ± 13% (RCP4.5), 58 ± 13% (RCP6.0), and 81 ± 12% (RCP8.5) by 2080–2099 (Koven et al., 2013; Slater & Lawrence, 2013). Permafrost variations among different permafrost subregions have also been projected using a diagnostic model driven by the outputs from multiple GCMs (Guo & Wang, 2016a).

These studies have mostly considered future permafrost variation based on GCMs. Although historical changes in permafrost are also referred in these studies, they lack accuracy because the results include a bias caused by simulated climate bias, which may amplify the rate of degradation of permafrost by 29% in the warmest case scenario of RCP8.5 (Lawrence et al., 2012). In addition, the results include unrealistic interannual variations in the extent of permafrost because GCMs are not designed to replicate variations in temperature for individual years. Some regional details in changes in the extent of permafrost cannot be captured as a result of the relatively coarse resolution of GCMs (usually ≥0.9° × 1.3°). An accurate estimation of the historical changes in permafrost is therefore required to compare or validate the results from GCMs. Research on historical changes in permafrost is useful in uncovering the response of permafrost to climate change and could help to advance our understanding of the future behavior of permafrost. For example, it has been shown that air temperatures in permafrost regions experienced a temporary increase during the 1930s and the 1940s (Guo, Li, & Hua, 2017). A study of the response of permafrost to this temporary increase in air temperatures would help our understanding of the range of increase in air temperatures required to cause the thawing of permafrost.

This study investigated historical changes in the extent of permafrost and the active layer thickness from 1901 to 2010 using the latest version of the Community Land Model (CLM4.5) driven by a set of new, high-resolution Climate Research Unit National Centers for Environmental Prediction (CRUNCEP) data set at a simulation resolution of 0.5° × 0.5°. The simulated results were validated based on observations of changes in soil temperatures and the active layer thickness and present-day extent of permafrost. In section 2, a description of the data, model, experimental design, and methods is provided. In section 3, the studied results with regard to validation of model, change in permafrost areas, and change in active layer thickness are presented. Discussions on potential sources of possible bias in the results are given in section 4, followed by conclusions of this study in section 5.

2. Data, Model, Experimental Design, and Methods

2.1. Data

CRUNCEP is a new, high-resolution atmospheric forcing data set (Viovy, 2011) combining the Climate Research Unit (CRU) TS3.2 monthly climatology with a resolution of 0.5° × 0.5° (Mitchell & Jones, 2005; Sun, 2017) and the National Centers for Environmental Prediction (NCEP) six-hourly reanalysis data with a resolution of 2.5° × 2.5° (Fan, Xie, & Xu, 2016; Gao, 2017; Kalnay et al., 1996). The CRUNCEP data set includes air temperature, precipitation, pressure, wind, specific humidity, downward short-wave radiation, and downward long-wave radiation. The data have a spatial resolution of 0.5° × 0.5° and a temporal resolution of 6 h over the time period of 1901–2010. Currently, there are five versions of CRUNCEP, version 4, that were used in this study. The data set has been used to drive the CLM for research on vegetation growth and evapotranspiration (Mao et al., 2013; Shi et al., 2013).

Daily soil temperature data from Russian meteorological stations were used to validate the simulated soil temperature (http://meteo.ru/english/climate/soil.php). The soil temperature was measured at depths of 0.02, 0.05, 0.1, 0.15, 0.2, 0.4, 0.6, 0.8, 1.2, 1.6, 2.4, and 3.2 m. The data at the depth of interest of 1 m were calculated using simple linear interpolation between known values. The data cover the period from 1963 to 2011, although the observation period varied between stations and some stations covered a shorter observation period. Only data from 1981 to 2009 were used in this study because the majority of stations had continuous data available for this period. Strict quality control was performed in creating the data so it is considered to be reliable.

Yearly active layer thickness observations were obtained from the Circumpolar Active Layer Monitoring network (Brown, Hinkel, & Nelson, 2000). These data cover the period of 1990–2015, but not all stations had records for the entire period. The data from 1996 to 2007 were used because most of the stations had continuous data during this period. These observations are available from http://www.gwu.edu/~calm/ and have previously been used to validate the results of climate models (Guo & Wang, 2016b; Koven et al., 2013; Lawrence et al., 2012).

The observations of the extent of permafrost used to validate the simulated present-day permafrost distribution were obtained from the *Circum-Arctic Map of Permafrost and Ground-Ice Conditions* (Brown et al., 1997). The data are available at http://nsidc.org/data/docs/fgdc/ggd318_map_circumarctic/index.html at a resolution of 0.5° × 0.5°. These data classify permafrost into continuous, discontinuous, isolated, and sporadic. However, it is argued that only continuous and discontinuous permafrost can be identified by climate models as a result of their coarse resolution (Burn & Nelson, 2006). Therefore, only these two types of permafrost were used for comparison with the simulated results. However, if the resolution of a climate model is sufficiently high, then other types of permafrost may be identified.

2.2. Model

The model used in this study was the latest version of the CLM, CLM4.5 (Oleson et al., 2013), which is an update of CLM4.0. A series of modifications has been performed in the CLM since version 3.0 to eliminate deficiencies in the simulation. The modifications relevant to permafrost simulation include an explicit treatment of soil freezing and thawing processes. The thawing begins when soil temperature is above 0°C and soil ice content is above 0, while the freezing begins when the soil temperature is below 0°C and soil liquid water content is above the maximum unfrozen water content. An expression for freezing point depression was used to calculate the maximum unfrozen water content to allow liquid water to coexist with ice over a wide range of soil temperatures below 0°C (Niu & Yang, 2006). The thermal and hydraulic properties of soil organic matter are represented to decrease the warm bias in the simulated soil temperature (Nicolsky et al., 2007). The soil has been extended to approximately 50 m depth, with a total of 15 layers, to account for thermal inertia from the cold, deep permafrost layers (Alexeev et al., 2007). The cold region hydrology process was improved from CLM4.0 to CLM4.5 for moderately dry near-surface organic soils (Swenson et al., 2012). These modifications have greatly improved the accuracy of frozen ground simulations and have made CLM4.5 one of the most sophisticated models for simulating the dynamics of permafrost (Koven et al., 2013; Lawrence et al., 2008; Lawrence et al., 2011).

2.3. Experimental Design

Six atmospheric forcing variables (air temperature, precipitation, pressure, wind, specific humidity, and downward short-wave radiation) required by the model as input data were obtained from the CRUNCEP data set. A global simulation was carried out with the CLMCRUNCEP chosen as the DATM (Data Atmosphere). The output of the model was set with a spatial resolution of 0.5° × 0.5° and a temporal resolution of 24 h. The simulation was initiated by cyclically running the model for 100 years with CRUNCEP data in 1979. The final model state was saved and taken as the initial conditions; the model was then cyclically run for 5 years with CRUNCEP data in 1901. The interannual change in soil temperature was $<$0.003°C at all soil levels when the initiation process ended, indicating that the model reached a steady state. The final state of initialization run was taken as the new initial conditions; the transient simulation was conducted for the period of 1901–2010.

2.4. Methods

Permafrost was defined as the ground where the monthly soil temperature in at least one soil layer in the upper 10 layers (3.8 m) remains below 0°C for 24 consecutive months (Lawrence et al., 2012). According to this definition, permafrost in this study refers to "near-surface permafrost." The active layer thickness was calculated as the maximum depth of thaw for permafrost over the course of a year using daily soil temperature data (Lawrence et al., 2008).

The model validation was based on a comparison between the simulated grid-mean results and individual site observations. A scale mismatch was therefore present in this validation, which may contribute to the bias between the simulations and observations. In spite of this, our comparison was based on the average of observations across all sites as the regional mean. This may moderate some of the effect of the scale mismatch on the validation.

The correlation coefficient and the Nash-Sutcliffe efficiency (NSE) were used to quantitatively assess the level of agreement between the simulations and observations (Nash & Sutcliffe, 1970). The NSE is calculated as follows:

$$\mathrm{NSE} = 1 - \frac{\sum_{t=1}^{T}\left(Q_{obs} - Q_{sim}\right)^2}{\sum_{t=1}^{T}\left(Q_{obs} - \overline{Q_{obs}}\right)^2}$$

where Q_{obs} represents observations, Q_{sim} represents simulations, and T represents the total samples. NSE is a normalized index that indicates how closely the plot of the simulated and observed results fits the 1:1 line. It has a range of $-\infty$ to 1; the simulated results are more accurate when the NSE is closer to 1 and the value 1 implies a perfect agreement of the simulated results with the observations.

The linear trend was the slope of the linear regression calculated by the least squares fitting method with a MATLAB function. The statistical significance of the trend was assessed by Student's t test.

Based on the different geographical characteristics controlling the formation of permafrost, permafrost can be classified into high-latitude and high-elevation permafrost subregions (Cheng & Wang, 1982). This study used the Tibetan Plateau to represent high-elevation permafrost region because typical and major high-elevation permafrost is distributed on the Tibetan Plateau. However, permafrost in some higher-latitude mountainous regions (e.g., the Alps) is also considered to be high-elevation permafrost. Given the great concern of permafrost-rich countries about the fate of their own permafrost as a result of local effects of thaw of permafrost, we classified the permafrost regions into four subregions with respect to the countries with large areas of permafrost: Russia, Canada, Alaska, and China.

3. Results

3.1. Validation of Model

The model reasonably captured the observed interannual change in soil temperature and active layer thickness (Figure 1). The change in the simulated soil temperature was in close agreement with observations at a depth of 1 m, with a correlation coefficient of 0.90 and an NSE of 0.78. The trend in the simulated soil temperature was 0.48°C decade^{-1}, which is close to, but slightly larger than, the trend of 0.45°C decade^{-1} in the observations. The simulated change in the active layer thickness also fits well with the observed values, with a correlation coefficient and an NSE of 0.73 and 0.21, respectively. The simulated trend was close to, but smaller than, the observed trend.

The simulated present-day (mean from 1981 to 2000) permafrost distribution largely corresponds to the observed distribution (Figure 1c). The discrepancies between the simulated and observed distribution of permafrost were mainly located on the eastern Tibetan Plateau. Permafrost in the eastern Tibetan Plateau cannot be fully identified in accordance with our definition of near-surface permafrost in the upper 3.8 m of soil as a result of the deep active layer thickness in this region. The simulated area of permafrost was 17.26×10^6 km^2, which compares reasonably with the observed area of 15.24×10^6 km^2 with a bias of 2.02×10^6 km^2. For different permafrost subregions, the simulated area of permafrost were 16.3 (high latitude), 0.97 (high elevation), 8.77 (Russia), 4.42 (Canada), 1.05 (Alaska), and 1.24 (China) $\times 10^6$ km^2, which are comparable with the observed area of 14.34 (high latitude), 0.90 (high elevation), 8.20 (Russia), 4.02 (Canada), 1.06 (Alaska), and 1.05 (China) $\times 10^6$ km^2, with biases of 1.96 (high latitude), 0.07 (high elevation), 0.57 (Russia), 0.40 (Canada), -0.01 (Alaska), and 0.19 (China) $\times 10^6$ km^2.

3.2. Change in Permafrost Areas

Permafrost in different regions of the Northern Hemisphere has experienced a statistically significant decrease in area from 1901 to 2009 (Figure 2). Over the entire permafrost region, the area of permafrost decreased by 0.06×10^6 km^2 decade^{-1} from 1901 to 2009. The decrease was more significant for the period

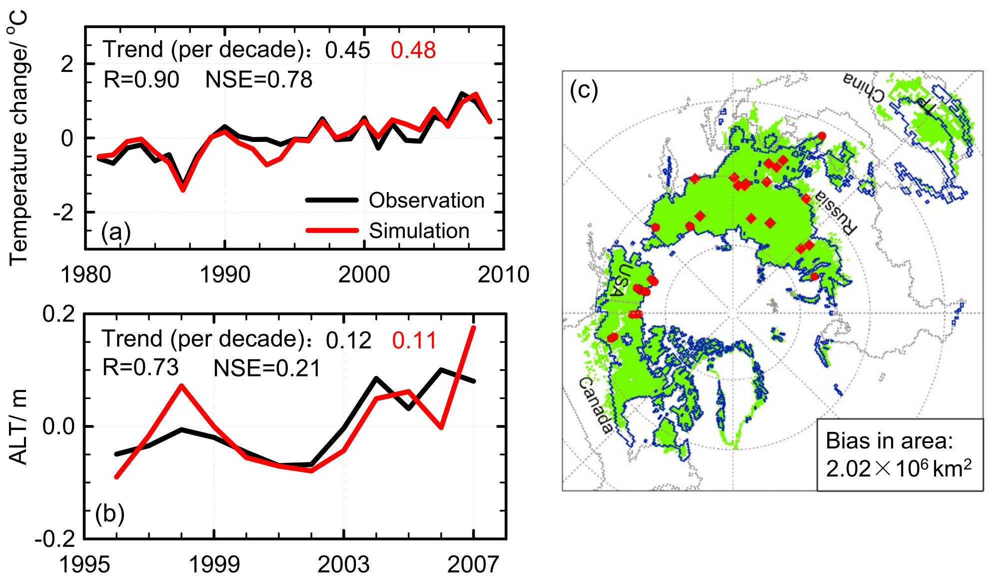

Figure 1. Comparison of the simulated and observed changes in (a) soil temperature at a depth of 1 m from 1981 to 2009 relative to the time period of 1981–2000 and (b) active layer thickness (ALT) from 1996 to 2007 relative to the time period of 1996–2007. Observations are averages among all stations. Linear trend, correlation coefficient (*R*), and Nash-Sutcliffe efficiency (NSE) of the simulations and observations are given. The observation stations for measurements of the soil temperature and ALT are shown as red rectangles and circles, respectively in Figure 1c. (c) Comparison of the simulated present-day extent of permafrost (*shaded color*) for 1981–2000 with observations (areas outlined in *blue*). The bias in the area between the simulated and observed results is given in the bottom right-hand corner of Figure 1c. The four countries considered here as subregions and the Tibetan Plateau (TP), containing mostly of permafrost, are outlined by gray dashed lines.

of 1979–2009, with a trend of -0.62×10^6 km^2 decade^{-1}. Permafrost subregions also uniformly showed a decrease in area from 1901 to 2009 and a more significant decrease from 1979 to 2009 (Figures 2b–2g).

There was a clear decrease in the extent of permafrost in response to increasing air temperatures over the entire permafrost region from the 1930s to the 1940s (Figure 2a). For the subregions of permafrost, high-latitude and high-elevation permafrost and permafrost in Canada and China showed a clear response to increasing air temperatures from the 1930s to the 1940s (Figures 2b–2g). Permafrost in Alaska appears to present a lagging response to increasing air temperatures, whereas permafrost in Russia does not show a clear response to increasing air temperatures. These results confirm that permafrost responds to increasing air temperatures, even if these persist for a relatively short period of time, except for the permafrost in Russia.

From a spatial perspective, permafrost decreased the most in the northern part of the Western Siberian Plain in Russia, the southern edge of the permafrost in Canada, and the northwestern Tibetan Plateau during the period of 2001–2010 relative to the 1900s (Figure 3a). A slight increase in the extent of permafrost was seen in northeastern China (Figure 3a). Although the changes were smaller, the places where either increases or decreases in permafrost occurred from 1935 to 1945 relative to the 1900s correspond well with those from 2001 to 2010 relative to the 1900s (Figure 3b). This indicates that these regions are likely to be the most sensitive to climate change. The decreases in permafrost during the periods 2001–2010 and 1935–1945 relative to the 1900s are caused by increasing local air temperature in each month of 24 consecutive months used to identify permafrost (not shown). The increase in permafrost are caused by increasing local summer precipitation rather than air temperature that show increase in all 24 consecutive months except for August (1935s–1900s) (Figures 4a and 4b). The increasing summer precipitation infiltrate into soil to result in an increase in soil liquid water (Figures 4c and 4d). The more liquid water produces a cool summer soil column because of its large thermal capacities (Figures 4e and 4f), which causes the increase in permafrost.

Comparisons of the rate of thawing of permafrost between different subregions showed that high-elevation permafrost thaws faster than high-latitude permafrost. Permafrost in China showed the fastest rate of thaw, followed by permafrost in Alaska, Russia, and Canada (Figure 5a). These differences are consistent with the predictions of Guo and Wang (2016a). The trends in the percentage decrease in area of permafrost in different regions had a statistically significantly positive correlation (correlation coefficient 0.93, exceeding the

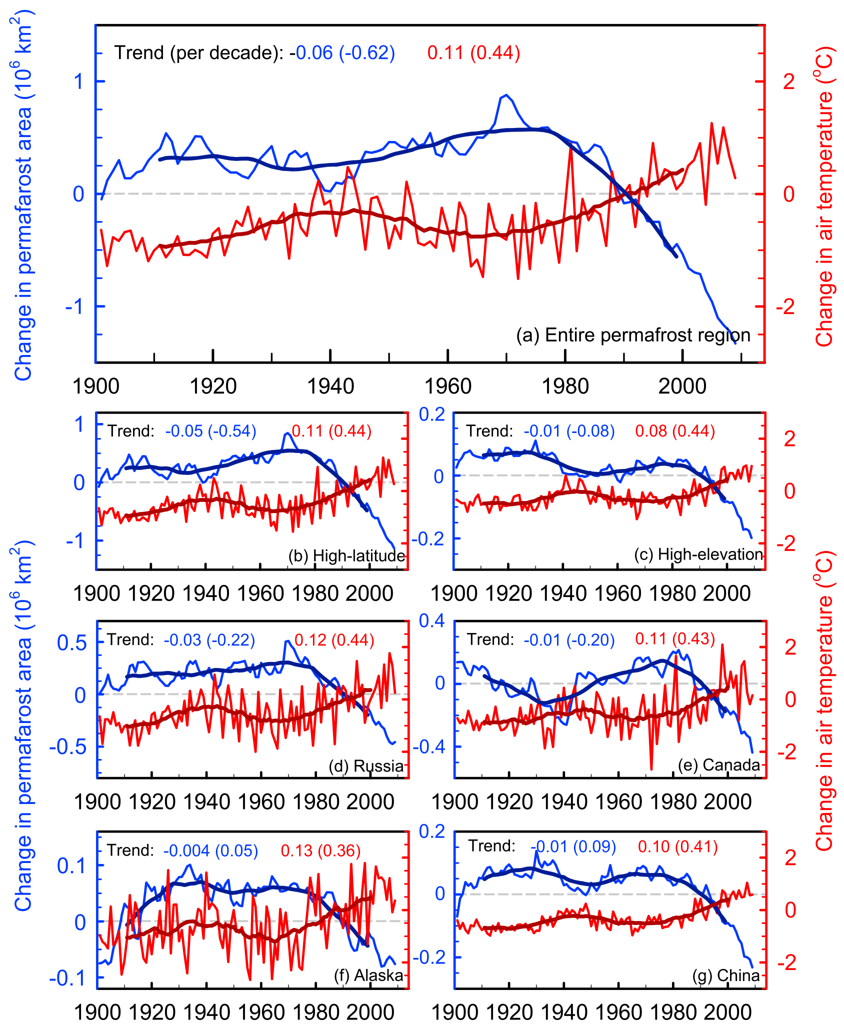

Figure 2. Changes in the areal extent of permafrost and air temperatures over (a) the entire region of permafrost in the Northern Hemisphere, (b) high-latitude regions with permafrost, (c) high-elevation regions with permafrost, and regions of permafrost in (d) Russia, (e) Canada, (f) Alaska, and (g) China from 1901 to 2009 relative to 1981–2000. The dark lines present the change smoothed using the 21 year moving average. Linear trends in permafrost area and air temperatures for the period of 1901–2009 are given at the top of each panel with trends for the period of 1979–2009 in parentheses.

significance level of 95%) with the sensitivity of permafrost in their own region to increasing air temperatures, but had a statistically significantly negative correlation (correlation coefficient 0.83, exceeding the significance level of 95%) with the rate of increase in air temperature in their own region (Figures 5b and 5c). This indicates that differences in the speed of thawing among different subregions are related to the sensitivity of permafrost in these areas to changes in air temperatures rather than to the amplitude of the change in air temperatures.

The sensitivity of permafrost to changes in air temperatures in different subregions are also related to their thermal conditions. Permafrost is defined as occurring when the soil temperature remains below 0°C for 24 consecutive months. In other words, as areas of permafrost warm and exceed 0°C, they can no longer be defined as permafrost. Given this definition, warmer permafrost more easily exceeds 0°C and becomes nonpermafrost than colder permafrost if temperature increases the same degree for both warmer and colder permafrost. This indicates that warm permafrost has a larger sensitivity to changes in air temperature than colder permafrost. According to the European Centre for Medium-Range Weather Forecasts Reanalysis Interim (ERA-Interim) data set (Dee et al., 2011), high-elevation permafrost is 6.77°C warmer than high-latitude permafrost. Permafrost in China (−2.39°C) is the warmest, followed by permafrost in Alaska (−6.54°C), Russia (−8.61°C), and Canada (−10.30°C). This corresponds to the speed of thawing of permafrost in these subregions.

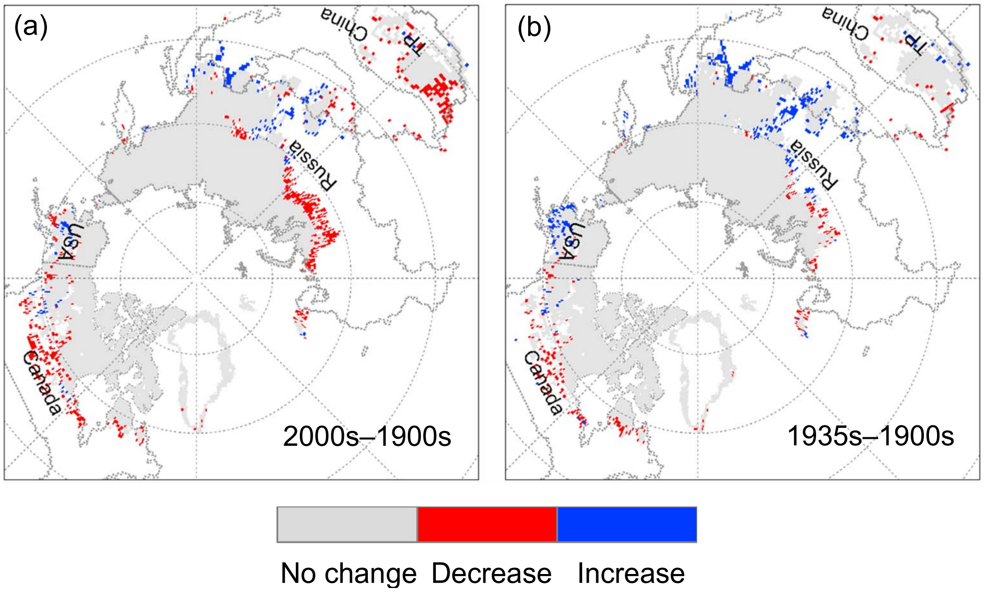

Figure 3. Changes in areal extent of permafrost in (a) the 2000s relative to the 1900s and (b) in the decade from 1935 to 1945 (1935s) relative to the 1900s. Four countries and the Tibetan Plateau (TP), consisting mostly of permafrost, are outlined by gray dashed lines.

3.3. Change in Active Layer Thickness

The active layer thickness over the entire permafrost region showed a statistically significantly increasing trend from 1901 to 2009 at a rate of 0.009 m decade^{-1}. The rate of increase intensified from 1979 to 2010 with a rate of 0.071 m decade^{-1} (Figure 6). A response to increasing air temperatures from about the 1930s to the 1940s can also be clearly seen in the change in the active layer thickness (Figure 6). The linear changes in the active layer thickness in permafrost subregions were similar to those over the entire permafrost region, except for Alaska, where the active layer thickness did not show a clear response to increasing air temperatures from about the 1930s to the 1940s (Figure 6).

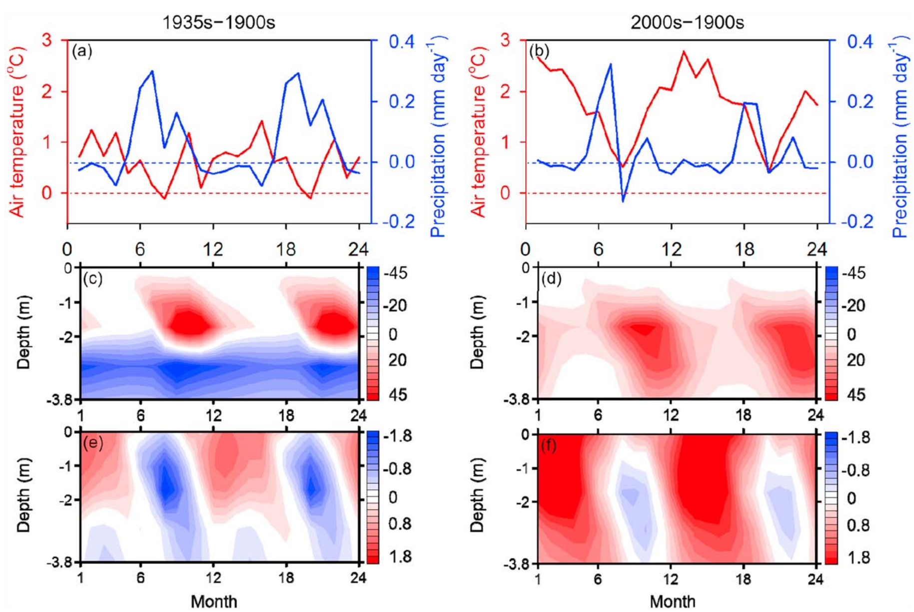

Figure 4. Differences in (a and b) air temperature (°C) (red), precipitation (mm day^{-1}) (blue), (c and d) soil liquid water (kg m^{-2}), and (e and f) soil temperature (°C) between the period 1935–1945 (1935s) and 1900s (Figures 4a, 4c, and 4e) and between the 2000s and 1900s (Figures 4b, 4d, and 4f), as averaged over the grid cells with increasing permafrost. The *x* axis represents the 24 consecutive months used to identify permafrost.

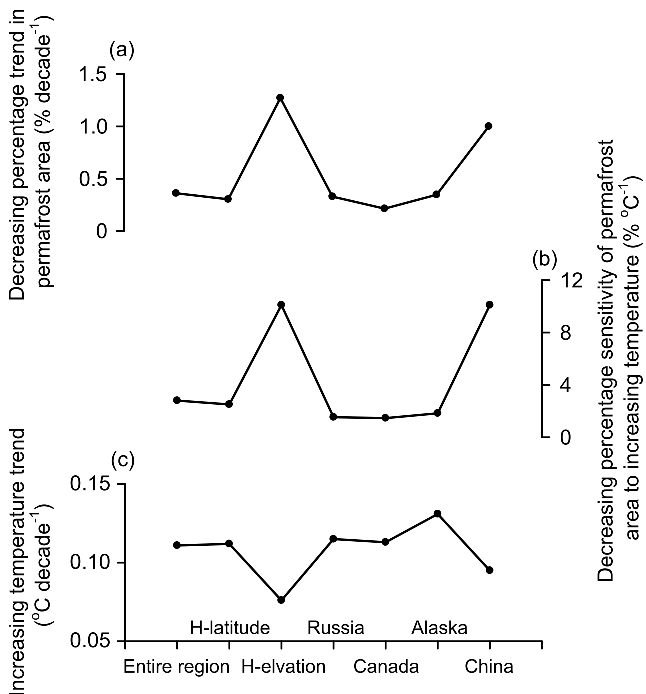

Figure 5. Relationship between (a) decreasing percentage trend in permafrost area (% decade^{-1}), (b) decreasing percentage sensitivity of permafrost area to increasing temperature (% °C^{-1}) (equivalent to percentage size of permafrost degradation when air temperature increase 1°C), and (c) increasing temperature trend (°C decade^{-1}) in the entire permafrost region (entire region), high-latitude (H-latitude) regions, high-elevation (H-elevation) regions, and in permafrost regions in Russia, Canada, Alaska, and China from 1901 to 2009. The correlation coefficient between the decreasing percentage trend in permafrost area and decreasing percentage sensitivity of permafrost area to increasing temperature is 0.93, whereas the correlation coefficient between the decreasing percentage trend in permafrost area and increasing temperature trend is −0.83. Both of correlation coefficients exceed the significance level of 95%.

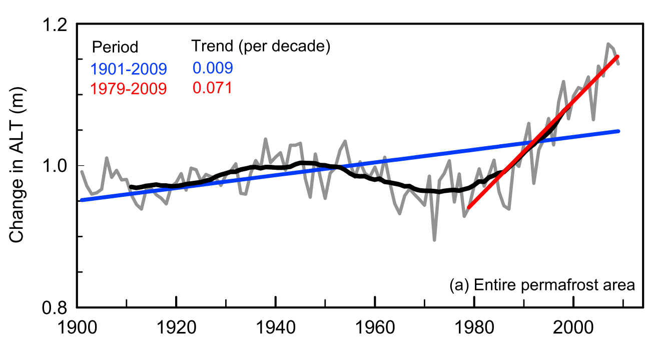

Figure 6. Simulated changes in the active layer thickness over (a) the entire region of permafrost in the Northern Hemisphere from 1901 to 2009 relative to 1981–2000. The blue and red lines represent regression lines during the periods 1901–2009 and 1979–2009, respectively. Linear trends (°C decade^{-1}) for the periods 1901–2009 and 1979–2009 are given in the top left of each panel.

From a spatial perspective, the majority of permafrost regions showed a significantly positive trend in active layer thickness during the period of 1901–2009. However, there were some regions where negative trends appeared, such as northwestern Canada, the northern edge of Greenland, and the northern part of the Siberian, Russia (Figure 7). Although the trends in active layer thickness during the period of 1979–2009 were distinctly larger, their spatial patterns were similar to those during the period of 1901–2009. Overall, the trends in active layer thickness decreased with increasing latitude, which is consistent with the future change in active layer thickness in the 2°C warming scenario reported by Guo and Wang (2016b).

4. Discussion

Biases in permafrost simulations are generally related to unrealistic representations of the physics of frozen ground in the models, low accuracy in the atmospheric data, and coarse resolution in the simulation. The CLM has undergone a series of improvements with respect to the process relevant to frozen ground, including the incorporation of soil organic matter, deepening of the soil layer, and corrections to the cold region hydrology scheme (Oleson et al., 2013). These improvements have enhanced the ability of the CLM to simulate frozen ground (Lawrence et al., 2012). A new higher-resolution atmospheric data set, CRUNCEP, has been developed as input data for land surface models (Viovy, 2011). CRUNCEP data and a simulation resolution of 0.5° × 0.5° were used in the latest version of the CLM (CLM4.5) to obtain a reliable estimate of historical changes in permafrost in the Northern Hemisphere. Longer-term series (29 years for soil temperature and 12 years for the active layer thickness) of the observed changes in permafrost were used to validate the simulated results rather than climatology observations that were generally used for validation in the papers with respect to simulation of frozen ground (e.g., Lawrence et al., 2012). The simulated results fitted well to observations, indicating that the simulated results are reasonable.

There was a relatively larger bias in the distribution of permafrost in the eastern Tibetan Plateau. This bias can be partially attributed to our definition of near-surface permafrost in the upper 3.8 m of soil. Using this definition, some of the permafrost cannot be identified because the thickness of the active layer (the permafrost table) is greater than 3.8 m in some permafrost regions of the Tibetan Plateau (Wu, Zhang, & Liu, 2010; Zhao et al., 2010). The simulated distribution of permafrost on the eastern Tibetan Plateau was closer to the observed distribution when the permafrost in deeper 4.7 m soil layers was considered (not shown). Surface data in the model may contribute to this bias to some extent. In our previous studies based on CLM4.0, a band with an unchanging active layer thickness was encountered as a result of bias in the soil organic matter content. The disappearance of the band in this study indicates an improvement in the data for soil organic matter. However, Han et al. (2015) and Gao, Shi, and Giorgi (2016) suggested that the vegetation cover within the CLM has some bias in the Tibetan Plateau, which may affect the transfer of water and heat into the soil and may further contribute to uncertainties in this simulation.

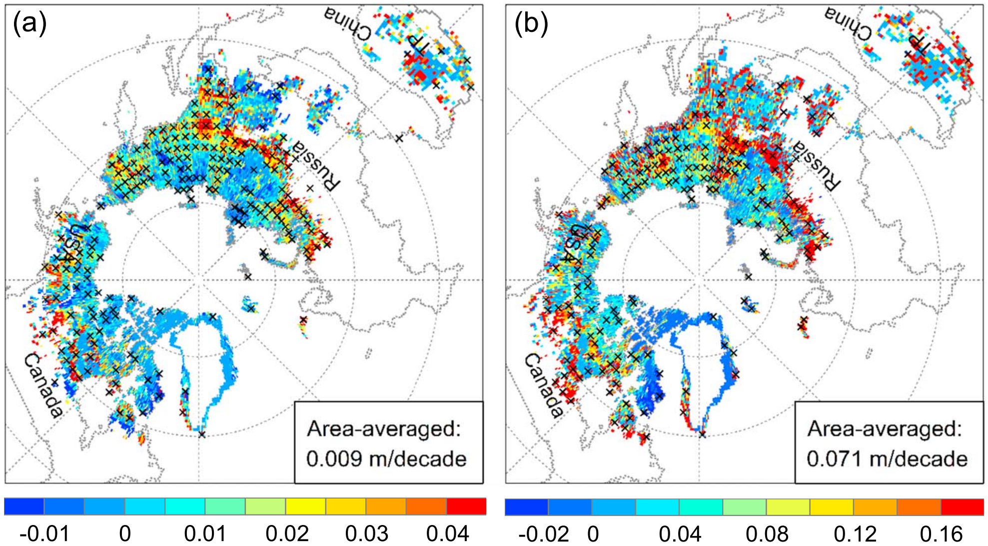

Figure 7. Distribution of trends in the simulated active layer thickness during the periods (a) 1901–2009 and (b) 1979–2009. Areas with a significant level >95% are denoted with plus symbols. The area-averaged trend in active layer thickness is given in the bottom right-hand corners of the panels. Four countries and the Tibetan Plateau (TP), consisting mostly of permafrost, are outlined by gray dashed lines.

An absence of excess ground ice in this model may be a source of uncertainty in this simulation. Previous studies have argued that the inclusion of excess ground ice may delay the speed of thawing of permafrost (Burn & Nelson, 2006). Lee et al. (2014) have shown that the inclusion of excess ice can delay the thawing of permafrost at 3 m depth by approximately 10 years in most regions with a high excess of ground ice. Excess ground ice has not been accounted for in the version of the CLM used in this study, and this contributes to the possible uncertainties in the simulation. The presence of excess ground ice can facilitate the prediction of thermal settlement hazard by this model—a hazard that seriously threatens the stabilization of engineering facilities underlain by permafrost and is caused by the degradation of permafrost (Guo & Wang, 2016b). It is therefore expected that excess ground ice will be incorporated into the next version of the CLM.

5. Conclusions

The dynamics of permafrost in the Northern Hemisphere were investigated using CLM4.5 driven by CRUNCEP data at a simulation resolution of 0.5° × 0.5°. Changes in the observed soil temperature and active layer thickness and the present-day extent of permafrost were captured well by this simulation, indicating that the simulated results are reasonable.

The area of permafrost decreased by 0.06 (0.62) × 10^6 km^2 $decade^{-1}$ and the active layer thickness increased by 0.009 (0.071) m $decade^{-1}$ during the period 1901–2009 (1979–2009). A clear decrease in the area of permafrost and an increase in the active layer thickness were found in response to increasing air temperatures from about the 1930s to the 1940s, indicating that permafrost is sensitive to even short-term warming of the Earth's climate.

High-elevation permafrost thaws faster than high-latitude permafrost. Permafrost in China had the fastest rate of thawing, followed by Alaska, Russia, and Canada. These regional differences in the rate of thawing are closely correlated to the sensitivity of permafrost in these regions to increases in air temperature, which is related to local thermal conditions.

These results provide an insight into the historical dynamics of permafrost in the Northern Hemisphere. They will be useful for understanding the response of permafrost to climate warming and can be used to validate the corresponding results from GCMs. The use of CLM4.5, the CRUNCEP data set, and a relatively high resolution are conducive to this simulation. Possible uncertainties in this study may be related to less accurate surface data and an absence of excess ground ice in the model. Previous simulations of permafrost have concentrated on the predication of the future degradation of permafrost based on GCMs (Anisimov & Nelson, 1996; Guo & Wang, 2016a; Koven et al., 2013; Lawrence et al., 2012; Stendel & Christensen, 2002;

Zhang et al., 2008). This study focused on the historical dynamics of permafrost based on a surface land model and atmospheric data. Future work is planned to examine the evolution of permafrost between typical historical cold and warm periods.

Acknowledgments
This research was jointly supported by the External Cooperation Program of BIC, the Chinese Academy of Sciences (134111KYSB20150016), the National Key R&D Program of China (2016YFA0600704), and the National Natural Science Foundation of China (41775076 and 41405087). We thank the National Snow and Ice Data Center (Boulder, CO, USA), which provided the *Circum-Arctic Map of Permafrost and Ground-Ice Conditions* (http://nsidc.org/data/docs/fgdc/ggd318_map_circumarctic/index.html).

References

Alexeev, V. A., Nicolsky, D. J., Romanovsky, V. E., & Lawrence, D. M. (2007). An evaluation of deep soil configurations in the CLM3 for improved representation of permafrost. *Geophysical Research Letters*, *34*, L09502. https://doi.org/10.1029/2007GL029536

Anisimov, O. A., & Nelson, F. E. (1996). Permafrost distribution in the Northern Hemisphere under scenarios of climate change. *Global and Planetary Change*, *14*(1-2), 59–72. https://doi.org/10.1016/0921-8181(96)00002-1

Brown, J., Ferrians, O. J., Jr, Heginbottom, J. A., & Melnikov, E. S. (1997). Circum-Arctic Map of Permafrost and Ground-Ice Conditions. U. S. Geol. Surv. in Cooperation with the Circum-Pacific Council for Energy and Mineral Resources, Circum-Pacific Map Series CP-45, scale 1:10,000,000, 1 sheet.

Brown, J., Hinkel, K., & Nelson, F. (2000). The Circumpolar Active Layer Monitoring (CALM) program: Research designs and initial results. *Polar Geography*, *24*, 165–258.

Burn, C. R., & Nelson, F. E. (2006). Comment on "A projection of severe near-surface permafrost degradation during the 21st century" by David M. Lawrence and Andrew G. Slater. *Geophysical Research Letters*, *33*, L21503. https://doi.org/10.1029/2006GL027077

Cheng, G. D., & Wang, S. L. (1982). On the zonation of high-altitude permafrost in China [in Chinese]. *Journal of Glaciology and Cryopedology*, *4*, 1–17.

Ciais, P., Sabine, C., Bala, G., Bopp, L., Brovkin, V., Canadell, J., … DeFries, R. (2013). Carbon and other biogeochemical cycles. In T. F. Stocker, et al. (Eds.), *Climate change 2013: The physical science basis. Contribution of working group I to the Fifth Assessment Report of the Intergovernmental Panel on Climate Change* (pp. 465–570). Cambridge, UK, and New York: Cambridge University Press.

Collins, M., Knutti, R., Arblaster, J., Dufresne, J.-L., Fichefet, T., Friedlingstein, P., … Gutowski, W. J. (2013). Long-term climate change: Projections, commitments and irreversibility. In T. F. Stocker, et al. (Eds.), *Climate change 2013: The physical science basis. Contribution of working group I to the Fifth Assessment Report of the Intergovernmental Panel on Climate Change*, (pp. 1029–1136). Cambridge, UK, and New York: Cambridge University Press.

Cuo, L., Zhang, Y., Bohn, T. J., Zhao, L., Li, J., Liu, Q., & Zhou, B. (2015). Frozen soil degradation and its effects on surface hydrology in the northern Tibetan Plateau. *Journal of Geophysical Research: Atmospheres*, *120*, 8276–8298. https://doi.org/10.1002/2015JD023193

Dee, D. P., Uppala, S. M., Simmons, A. J., Berrisford, P., Poli, P., Kobayashi, S., … Balmaseda, M. A. (2011). The ERA-Interim reanalysis: Configuration and performance of the data assimilation system. *Quarterly Journal of the Royal Meteorological Society*, *137*(656), 553–597. https://doi.org/10.1002/qj.828

Fan, K., Xie, Z., & Xu, Z. (2016). Two different periods of high dust weather frequency in northern China. *Atmospheric and Oceanic Science Letters*, *9*(4), 263–269. https://doi.org/10.1080/16742834.2016.1176300

Gao, Y. (2017). Shift of the principal mode of Pan-Asian monsoon summer precipitation in terms of spatial pattern. *Atmospheric and Oceanic Science Letter*, *10*(3), 221–227. https://doi.org/10.1080/16742834.2017.1294460

Gao, X. J., Shi, Y., & Giorgi, F. (2016). Comparison of convective parameterizations in RegCM4 experiments over China with CLM as the land surface model. *Atmospheric and Oceanic Science Letter*, *9*(4), 246–254. https://doi.org/10.1080/16742834.2016.1172938

Guo, D. L., Li, D., & Hua, W. (2017). Quantifying air temperature evolution in the permafrost region from 1901 to 2014. *International Journal of Climatology*. https://doi.org/10.1002/joc.5161

Guo, D. L., & Sun, J. Q. (2015). Permafrost thaw and associated settlement hazard onset timing over the Qinghai-Tibet engineering corridor. *International Journal of Disaster Risk Sciences*, *6*(4), 347–358. https://doi.org/10.1007/s13753-015-0072-3

Guo, D. L., & Wang, H. J. (2012). The significant climate warming in the northern Tibetan Plateau and its possible causes. *International Journal of Climatology*, *32*, 1775–1781.

Guo, D. L., & Wang, H. J. (2013). Simulation of permafrost and seasonally frozen ground conditions on the Tibetan Plateau, 1981–2010. *Journal of Geophysical Research: Atmospheres*, *118*, 5216–5230. https://doi.org/10.1002/jgrd.50457

Guo, D. L., & Wang, H. J. (2016a). CMIP5 permafrost degradation projection: A comparison among different regions. *Journal of Geophysical Research: Atmospheres*, *121*, 4499–4517. https://doi.org/10.1002/2015JD024108

Guo, D. L., & Wang, H. J. (2016b). Permafrost degradation and associated ground settlement estimation under 2°C global warming. *Climate Dynamics*, *49*(7-8), 2569–2583. https://doi.org/10.1007/s00382-016-3469-9

Guo, D. L., Wang, H. J., & Li, D. (2012). A projection of permafrost degradation on the Tibetan Plateau during the 21st century. *Journal of Geophysical Research*, *117*, D05106. https://doi.org/10.1029/2011JD016545

Guo, D. L., Yang, M. X., & Wang, H. J. (2011a). Characteristics of land surface heat and water exchange under different soil freeze/thaw conditions over the central Tibetan Plateau. *Hydrological Processes*, *25*(16), 2531–2541. https://doi.org/10.1002/hyp.8025

Guo, D. L., Yang, M. X., & Wang, H. J. (2011b). Sensible and latent heat flux response to diurnal variation in soil surface temperature and moisture under different freeze/thaw soil conditions in the seasonal frozen soil region of the central Tibetan Plateau. *Environment and Earth Science*, *63*(1), 97–107. https://doi.org/10.1007/s12665-010-0672-6

Han, Z., Gao, X., Shi, Y., Wu, J., Wang, M., & Giorgi, F. (2015). Development of Chinese high resolution land cover data for the RegCM4/CLM and its impact on regional climate simulation [in Chinese]. *Journal of Glaciology and Geocryology*, *37*, 857–866.

Kalnay, E., Kanamitsu, M., Kistler, R., Collins, W., Deaven, D., Gandin, L., … Saha, S. (1996). The NCEP/NCAR 40-year reanalysis project. *Bulletin of the American Meteorological Society*, *77*(3), 437–471. https://doi.org/10.1175/1520-0477(1996)077%3C0437:TNYRP%3E2.0.CO;2

Koven, C. D., Riley, W. J., & Stern, A. (2013). Analysis of permafrost thermal dynamics and response to climate change in the CMIP5 Earth System Models. *Journal of Climate*, *26*(6), 1877–1900. https://doi.org/10.1175/JCLI-D-12-00228.1

Lawrence, D. M., Oleson, K. W., Flanner, M. G., Thornton, P. E., Swenson, S. C., Lawrence, P. J., … Slater, A. G. (2011). Parameterization improvements and functional and structural advances in version 4 of the Community Land Model. *Journal of Advances in Modeling Earth Systems*, *3*(3), M03001. https://doi.org/10.1029/2011MS000045

Lawrence, D. M., Slater, A. G., Romanovsky, V. E., & Nicolsky, D. J. (2008). Sensitivity of a model projection of near-surface permafrost degradation to soil column depth and representation of soil organic matter. *Journal of Geophysical Research*, *113*, F02011. https://doi.org/10.1029/2007JF000883

Lawrence, D. M., Slater, A. G., & Swenson, S. C. (2012). Simulation of present-day and future permafrost and seasonally frozen ground conditions in CCSM4. *Journal of Climate*, *25*(7), 2207–2225. https://doi.org/10.1175/JCLI-D-11-00334.1

Lee, H., Swenson, S. C., Slater, A. G., & Lawrence, D. M. (2014). Effects of excess ground ice on projections of permafrost in a warming climate. *Environmental Research Letters*, *9*(12), 124006. https://doi.org/10.1088/1748-9326/9/12/124006

Li, Q., & Chen, H. S. (2013). Variation of seasonal frozen soil in East China and their association with monsoon activity under the background of global warming [in Chinese]. *Climate Change Research Letters*, *02*(02), 47–53. https://doi.org/10.12677/CCRL.2013.22008

Liljedahl, A. K., Boike, J., Daanen, R. P., Fedorov, A. N., Frost, G. V., Grosse, G., … Zona, D. (2016). Pan-Arctic ice-wedge degradation in warming permafrost and its influence on tundra hydrology. *Nature Geoscience*, *9*(4), 312–318. https://doi.org/10.1038/ngeo2674

Liu, Y., & Jiang, D. (2016). Mid-Holocene permafrost: Results from CMIP5 simulations. *Journal of Geophysical Research: Atmospheres*, *121*, 221–240. https://doi.org/10.1002/2015JD023837

Mao, J., Shi, X., Thornton, P. E., Hoffman, F. M., Zhu, Z., & Myneni, R. B. (2013). Global latitudinal-asymmetric vegetation growth trends and their driving mechanisms: 1982–2009. *Remote Sensing*, *5*(3), 1484–1497. https://doi.org/10.3390/rs5031484

Mitchell, T. D., & Jones, P. D. (2005). An improved method of constructing a database of monthly climate observations and associated high-resolution grids. *International Journal of Climatology*, *25*(6), 693–712. https://doi.org/10.1002/joc.1181

Mu, C., Zhang, T., Wu, Q., Peng, X., Cao, B., Zhang, X., … Cheng, G. (2015). Editorial: Organic carbon pools in permafrost regions on the Qinghai–Xizang (Tibetan) Plateau. *The Cryosphere*, *9*(2), 479–486. https://doi.org/10.5194/tc-9-479-2015

Nash, J. E., & Sutcliffe, J. V. (1970). River flow forecasting through conceptual models. Part I: A discussion of principles. *Journal of Hydrology*, *10*(3), 282–290. https://doi.org/10.1016/0022-1694(70)90255-6

Nelson, F. E., Anisimov, O. A., & Shiklomanov, N. (2002). Climate change and hazard zonation in the circum-Arctic permafrost regions. *Natural Hazards*, *26*(3), 203–225. https://doi.org/10.1023/A:1015612918401

Nicolsky, D. J., Romanovsky, V. E., Alexeev, V. A., & Lawrence, D. M. (2007). Improved modeling of permafrost dynamics in a GCM land-surface scheme. *Geophysical Research Letters*, *34*, L08501. https://doi.org/10.1029/2007GL029525

Niu, G. Y., & Yang, Z. L. (2006). Effects of frozen soil on snowmelt runoff and soil water storage at a continental scale. *Journal of Hydrometeorology*, *7*(5), 937–952. https://doi.org/10.1175/JHM538.1

Oleson, K., Lawrence, D. M., Bonan, G. B., Drewniak, B., Huang, M., Koven, C. D., … Li, F. (2013). Technical description of version 4.5 of the Community Land Model (CLM), NCAR Tech. Note NCAR/TN-503+STR (434 pp.). Boulder, CO: National Center for Atmospheric Research.

Qin, D. H., Zhou, B. T., & Xiao, C. D. (2014). Progress in studies of cryospheric changes and their impacts on climate of China. *Journal of Meteorological Research*, *28*(5), 732–746. https://doi.org/10.1007/s13351-014-4029-z

Schuur, E., McGuire, A. D., Schädel, C., Grosse, G., Harden, J. W., Hayes, D. J., … Vonk, J. E. (2015). Climate change and the permafrost carbon feedback. *Nature*, *520*(7546), 171–179. https://doi.org/10.1038/nature14338

Shi, X., Mao, J., Thornton, P. E., & Huang, M. (2013). Spatiotemporal patterns of evapotranspiration in response to multiple environmental factors simulated by the Community Land Model. *Environmental Research Letters*, *8*(2), 024012. https://doi.org/10.1088/1748-9326/8/2/024012

Slater, A. G., & Lawrence, D. M. (2013). Diagnosing present and future permafrost from climate models. *Journal of Climate*, *26*(15), 5608–5623. https://doi.org/10.1175/JCLI-D-12-00341.1

Stendel, M., & Christensen, J. (2002). Impact of global warming on permafrost conditions in a coupled GCM. *Geophysical Research Letters*, *29*(13), 1632. https://doi.org/10.1029/2001GL014345

Sun, B. (2017). Seasonal evolution of the dominant modes of the Eurasian snowpack and atmospheric circulation from autumn to the subsequent spring and the associated surface heat budget. *Atmospheric and Oceanic Science Letters*, *10*(3), 191–197. https://doi.org/10.1080/16742834.2017.1286226

Swenson, S. C., Lawrence, D. M., & Lee, H. (2012). Improved simulation of the terrestrial hydrological cycle in permafrost regions by the Community Land Model. *Journal of Advances in Modeling Earth Systems*, *4*(3), M08002. https://doi.org/10.1029/2012MS000165

Tian, Z. P., & Jiang, D. B. (2015). Revisiting mid-Holocene temperature over China using PMIP3 simulations. *Atmospheric and Oceanic Science Letters*, *8*, 358–364.

Viovy, N. (2011). CRUNCEP dataset. Retrieved from http://dods.extra.cea.fr/data/p529viov/cruncep/readme.htm

Wu, Q. B., Zhang, T. J., & Liu, Y. Z. (2010). Permafrost temperatures and thickness on the Qinghai-Tibet Plateau. *Global and Planetary Change*, *72*(1-2), 32–38. https://doi.org/10.1016/j.gloplacha.2010.03.001

Yang, M. X., Nelson, F., Shiklomanov, N., Guo, D. L., & Wan, G. (2010). Permafrost degradation and its environmental effects on the Tibetan Plateau: A review of recent research. *Earth Science Reviews*, *103*(1-2), 31–44. https://doi.org/10.1016/j.earscirev.2010.07.002

Yi, S., Wang, X., Qin, Y., Xiang, B., & Ding, Y. (2014). Responses of alpine grassland on Qinghai–Tibetan plateau to climate warming and permafrost degradation: A modeling perspective. *Environmental Research Letters*, *9*(7), 074014. https://doi.org/10.1088/1748-9326/9/7/074014

Zhang, T., Barry, R. G., Knowles, K., Heginbottom, J. A., & Brown, J. (1999). Statistics and characteristic of permafrost and ground-ice distribution in the Northern Hemisphere. *Polar Geography*, *23*(2), 132–154. https://doi.org/10.1080/10889379909377670

Zhang, Y., Chen, W., & Riseborough, D. W. (2008). Transient projections of permafrost distribution in Canada during the 21st century under scenarios of climate change. *Global and Planetary Change*, *60*(3-4), 443–456. https://doi.org/10.1016/j.gloplacha.2007.05.003

Zhao, L., Wu, Q. B., Marchenko, S. S., & Sharkhuu, N. (2010). Thermal state of permafrost and active layer in central Asia during the international polar year. *Permafrost and Periglacial Processes*, *21*(2), 198–207. https://doi.org/10.1002/ppp.688

Zhou, B. T., Xu, Y., Wu, J., Dong, S., & Shi, Y. (2016). Changes in temperature and precipitation extreme indices over China: Analysis of a high-resolution grid dataset. *International Journal of Climatology*, *36*(3), 1051–1066. https://doi.org/10.1002/joc.4400